ELSEVIER

Ceramics International 31 (2005) 965–971

CERAMICS INTERNATIONAL

www.elsevier.com/locate/ceramint

Electrical, thermal and catalytic properties of CeO_2–$Sm_{0.5}Ti_{0.5}O_{1.75}$ ceramics

Serguei Koutcheiko*, Yeong Yoo, Isobel Davidson

Institute for Chemical Process and Environmental Technology, National Research Council Canada, Ottawa, ON, Canada K1A 0R6

Received 20 May 2004; received in revised form 16 September 2004; accepted 9 October 2004
Available online 13 January 2005

Abstract

The electrical conductivity of the ceramic composite, $(CeO_2)_{1-x}(Sm_{0.5}Ti_{0.5}O_{1.75})_x$, where $0 \leq x \leq 0.2$ has been investigated in air and in forming gas (8% H_2 + 92% Ar). Complex impedance measurements indicated that the pyrochlore phase affected the grain-boundary conduction in these ceramic composites. The grain-boundary resistance decreased with increasing dopant content. The thermal behavior of these ceramics under reducing conditions was also investigated. Evaluations of catalytic behaviour showed that the addition of 5 mol% of pyrochlore phase to ceria improved the catalytic activity for steam reforming of methane.

Keywords: A. Sintering; C. Electrical conductivity; D. CeO_2; E. Fuel cells

1. Introduction

Although Ni-YSZ cermet is considered, so far, to be the most reliable candidate as the anode material for solid oxide fuel cells (SOFC), many studies seeking an alternative material for the anode have been made [1]. Recently, reports have been published in which perovskite anodes mixed with CeO_2 were successfully tested [2]. Both doped and undoped ceria are mixed ionic and electronic conductors at low oxygen partial pressure and are considered to be promising SOFC anode components [3,4]. In two previous studies, the ability of ceria to suppress carbon deposition in methane-rich atmospheres allowed cell operation on at a low steam-to-carbon ratios [5,6]. Ceria itself is a very interesting component of modern catalytic systems. It was found that due to its oxygen storage ability CeO_2 serves as unusual oxidant for oxidation of CH_4 into H_2 and CO. It has been shown to promote precious-metal catalysts for the water-gas-shift reaction [7]. It is known also, that ceria-based oxides are reduced under reductive atmospheres making them electronically conductive. The magnitude of electrical conductivity and the stability under reductive atmospheres for ceria-based oxides are greatly dependent on the kind and quantity of doping elements [4]. The volume of ceria depends drastically on the nature of the surrounding gaseous atmosphere. Transition of Ce^{4+} to Ce^{3+} expands the ceria lattice under reducing conditions. Oxidation of reduced ceria is a strongly exothermic process and takes place at low temperatures. It has been reported that this may result in the formation of cracks at the electrode–electrolyte interface or delamination of the electrode from the surface of the electrolyte [8].

In the present work the electrical, thermal, and catalytic properties of ceria doped with a pyrochlore phase, $Sm_2Ti_2O_7$, are investigated. The pyrochlore structure type is closely related to the fluorite type structure. The substitution of two A^{3+} and two B^{4+} cations for four M^{4+} cations in the parent fluorite requires the presence of seven rather than eight oxygen ions per formula unit. One-eighth of the anion sites in pyrochlore must be vacant. Oxygen ion conductivity that results from the disorder in the anion array rapidly increases with increasing temperature. Addition of or doping with lower valent cations are known to decrease the expansion and contraction of ceria during reduction and oxidation. It is also known that thermal

* Corresponding author. Fax: +1 613 991 2384.
E-mail address: serguei.koutcheiko@nrc.ca (S. Koutcheiko).

0272-8842/$30.00
doi:10.1016/j.ceramint.2004.10.010

properties of ceria can be adjusted by adding a significant fraction of a second phase [8,9]. Pyrochlore-type oxides have been shown previously to be promising components of catalysts for methane reforming and formation of synthesis gas [10].

2. Experimental

As starting materials CeO_2 (99.9%, Aldrich, Milwaukee, WI), Sm_2O_3 (99.9%, Aldrich, Milwaukee, WI), and TiO_2 (99.8%, Alfa Aesar, Ward Hill, MA) were used. $Sm_{0.5}Ti_{0.5}O_{1.75}$ (STO) was synthesized by a solid-state reaction of Sm_2O_3 and TiO_2 at 1400 °C for 10 h in air. Ceria and STO were mixed in ratios according to the formula $1 - x(CeO_2)$–xSTO, where $0 \leq x \leq 0.2$, and ball milled for 24 h in ethanol in a plastic container using zirconia balls. These mixtures were then calcined at 1300 °C for 5 h in air.

Powder X-ray diffraction measurements on the samples were performed to identify their crystal structure, lattice parameters, and phase composition on a Bruker D8 Advanced X-ray diffractometer (Bruker AXS Gmbh, Karlsruhe, Germany) with Cu Kα radiation.

A.c. impedance measurements using a two electrode configuration were made with an impedance/gain-phase analyzer Solartron SI 1260A and an electrochemical interface Solartron SI 1287 (Solartron Group Ltd., Farnborough, England) over the frequency range from 10^6 to 10^{-2} Hz. Measurements were performed on rectangular bars 4 mm × 4 mm × 19 mm sintered at 1300 °C for 10 h in air. Gold electrodes were formed on both end surfaces by brush painting of gold paste (Ferro 4007) and firing at 900 °C for 1 h. A.c. impedance measurements were made in air between 600 and 900 °C.

The electrical conductivity was measured using the conventional dc four-probe technique in air and in forming gas (8% H_2 in Ar) in the range 650–900 °C for both decreasing and increasing temperatures. In order to decrease the equilibration time in forming gas the samples with lower density (∼75%) were used. Two Pt voltage probes with a spacing of 10 mm were formed at positions 4.5 mm apart from both ends by winding Pt leads.

The microstructures of sintered ceramics were observed under SEM Hitachi S-4800 equipped with analyzer INCAx-singht. An appropriate thermal etching is needed for SEM to reveal the grains and grain boundaries in the samples. Average grain size was determined by Mendelson method [11].

The bulk density measurements were determined from the mass of the specimen and its geometrical dimensions.

Thermal expansion coefficients (TECs) and thermal expansion behavior under reducing conditions were measured using a Setsys Evolution thermo mechanical analyzer (Setaram, Caluire, France) over the temperature range of 25–950 °C under flowing forming gas (flowing rate 40 cm^3/min) at heating and cooling rates of 3 °C/min. The TECs were calculated for the temperature range of 400–800 °C from the cooling data. A fused silica rod was used as a reference.

For the catalytic tests $(CeO_2)_{1-x}(STO)_x$ powders calcined at 1300 °C were ball milled for 24 h, then pressed into pellets of 5 mm diameter and 3 mm thickness using polyvinylalcohol containing solution as a binder solution. The pressed pellets were sintered at 1200 °C for 1 h in forming gas to produce porosity of about 40–45% by volume. For each test, fresh catalyst (∼0.5 g) was put in a quartz tube of 25 cm length and two quartz wool plugs were inserted on both sides of the sample. All gas input and output lines of the reactor were heated to 100 °C to prevent water absorption. A mixture of 5% CH_4 and 95% of Ar bubbled through water (50 °C) was used as the feed gas. The feed rate was kept constant at 30 cm^3/min by monitoring with a mass-flow meter. The measurements were performed under dynamic conditions in the range 100–950 °C at the heating rate of 5 °C/min. Both the reaction products and the inlet gas mixtures were analyzed using a quadruple mass spectrometer QME 200 (Balzers, Hudson, NH) calibrated for CH_4, Ar, CO, CO_2, and H_2 with a standard gas mixture.

3. Results and discussion

3.1. XRD analysis and electrical conductivity measurements

The X-ray diffraction patterns of $(CeO_2)_{1-x}$–STO_x ceramics sintered in air consisted of two phases – fluorite and pyrochlore (see Fig. 1). The cell parameters of doped CeO_2 vary in the range 5.4121 ± 0.0006 Å and are essentially unchanged from that of pure CeO_2 (a = 5.4109 Å, [12]), indicating very low solubility of STO in the matrix.

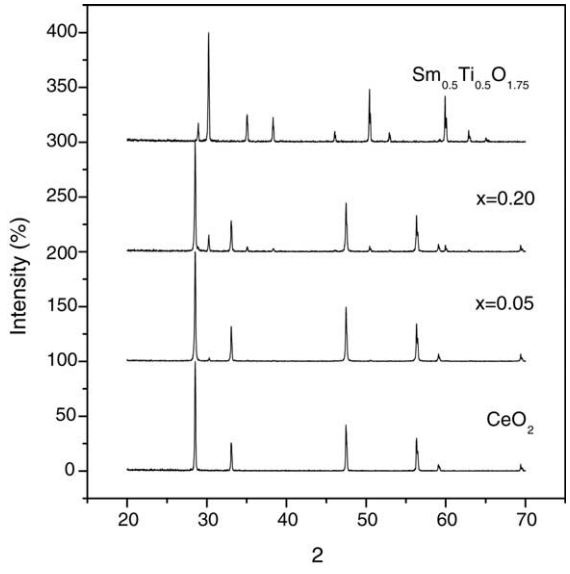

Fig. 1. X-ray diffraction patterns for $(CeO_2)_{1-x}(STO)_x$ ceramics sintered at 1300 °C.

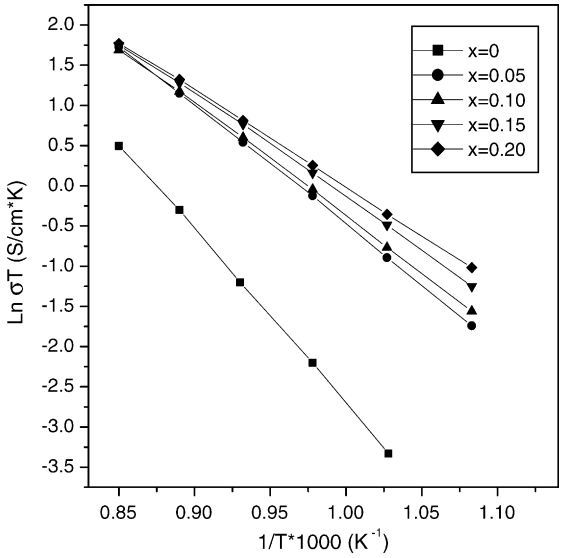

Fig. 2. Conductivity plots ln σT vs. $1/T$ for $(CeO_2)_{1-x}(STO)_x$ ceramics determined with four-probe method in air.

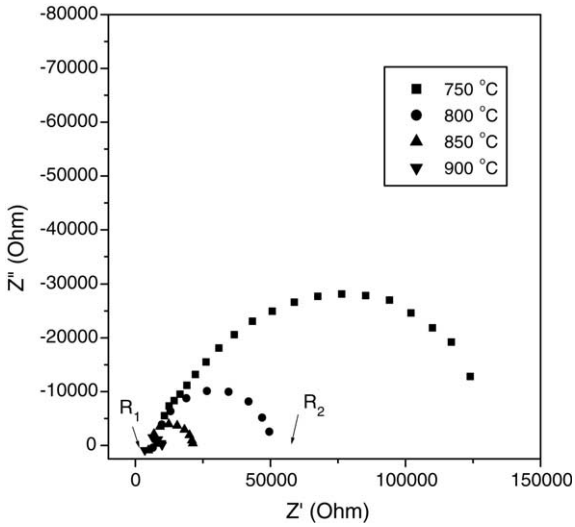

Fig. 3. The ac complex impedance plots for CeO_2 ceramic obtained in air.

The temperature dependence of the electrical conductivity in air of the $(CeO_2)_{1-x}$–$(STO)_x$ samples is shown in Fig. 2. Conductivity plots ln σT versus $1/T$ exhibited linear relations, indicating that there is no change in the activation energy within the temperature range of 650–900 °C. The conductivity measured in air was assumed to be predominantly ionic. Doped samples showed higher conductivity than pure CeO_2. The conductivity values were almost independent of x at high temperatures where the influence of grain boundaries is negligible. These data are in a good agreement with the XRD data and prove that there is very limited solubility of pyrochlore in CeO_2. At the same time the activation energy E_a decreased as STO content increased (Table 1). The ceramic with $x = 0.2$ showed the highest conductivity at 650 °C despite having the highest content of pyrochlore as a secondary phase.

To further investigate the influence of STO on the oxygen ionic conductivity of $(CeO_2)_{1-x}$–STO_x materials, investigations by ac impedance spectroscopy at different temperatures was used. Nyquist plots for pure CeO_2 recorded in the range 750–900 °C are presented in Fig. 3 (the electrode–ceramic interface arc has been eliminated). The impedance spectrum exhibited only one arc, which can be related to the contribution from grain boundaries [13]. The resistance R_1 is a grain resistance and it can be obtained from the intersections on the real axis of the high frequency side of the arc after fitting circle. The resistance R_2, from the intersection on the real axis of the low frequency side of the arc, corresponds to dc resistance measured by four-probe method. It can be seen that the grain-boundary arc is highly depressed. It indicates a non-Debye relaxation with significant degree of heterogeneity in the conduction path. The degree of heterogeneity, however, remains nearly the same in the temperature range between 750 and 900 °C (the depression angle ≅45°). The size or diameter of the arc decreases and, therefore, grain-boundary contribution decreases with increasing temperature. The electrical conductivity of undoped CeO_2 was calculated based on R_2 values and activation energy E_a was found to be 1.9 eV that is very close to the value obtained from four-probe measurements (see Table 1). The conductivity within the grains of CeO_2 calculated from R_1 values increased with increasing temperature and was found to be 3.1×10^{-3} S/cm at 900 °C. The activation energy E_a^{gr} in the range 800–900 °C was found to be 0.69 eV, which is in a good agreement with results obtained by Wang and Nowick [14] for 99.95% purity CeO_2 and somewhat lower than the activation energy for migration of oxygen vacancies in CeO_2 −0.76 eV [15]. The discrepancy is, probably, due to electronic conductivity induced at high temperature.

Table 1
The electrical properties of $(CeO_2)_{1-x}(STO)_x$ ceramics under air and forming gas atmospheres

Composition (x)	Air			Forming gas (92% Ar–8% H_2)		
	Density (g/cm^3)	σ at 700 °C (S/cm)	E_a (eV)	Density (g/cm^3)	σ at 700 °C (S/cm)	E_a (eV)
0	6.80	3.7×10^{-5}	1.86	5.01	0.72	0.45
0.05	6.75	4.2×10^{-4}	1.29	4.81	0.36	0.48
0.10	6.58	4.9×10^{-4}	1.21	4.97	0.25	0.47
0.15	6.37	6.3×10^{-4}	1.11	4.77	0.21	0.49
0.20	6.23	7.2×10^{-4}	1.05	4.76	0.11	0.51

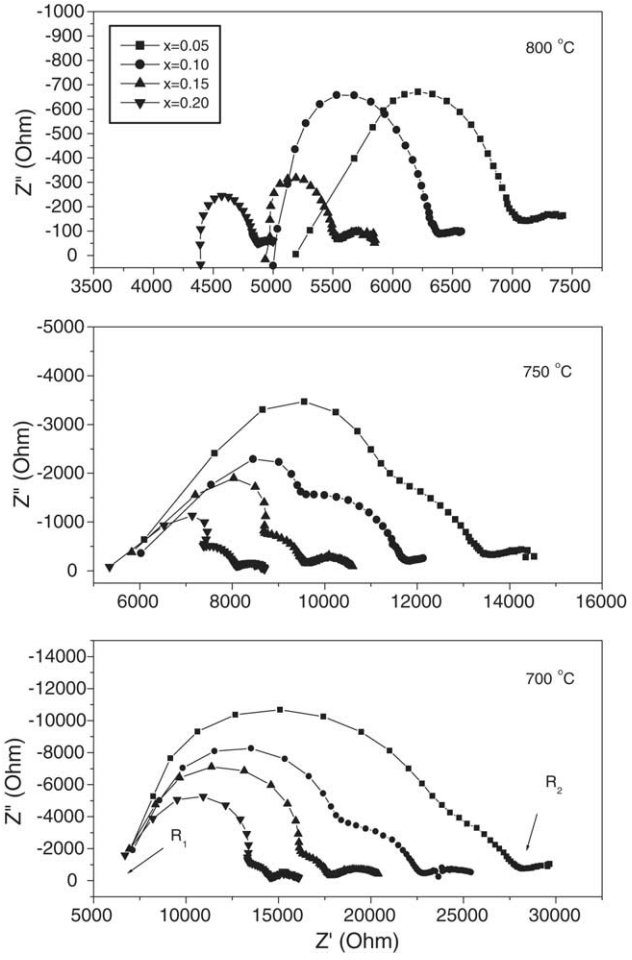

Fig. 4. The ac complex impedance plots for $(CeO_2)_{1-x}(STO)_x$ ceramics obtained in air.

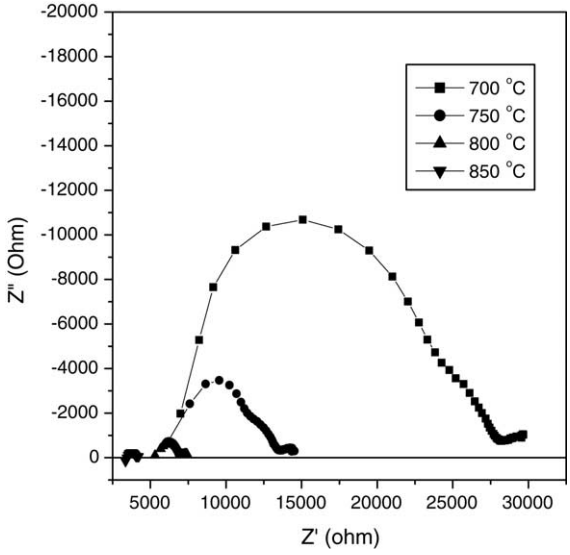

Fig. 5. The ac complex impedance plots for $(CeO_2)_{0.95}(STO)_{0.05}$ ceramics as a function of temperature.

The results of ac impedance measurement of STO-doped ceramics are presented in Fig. 4. In this case the grain-boundary effect is more complex. The high frequency intercept of ac complex impedance plots has been usually associated with grain conductivity. In our case the ceria–ceria grain-boundary arc and the arc associated with STO content are heavily overlapping and for simplicity of qualitative evaluation of the spectra they can be considered as a total ''grain-boundary effect''. The spectra at 700–750 °C consist of three distinct arcs. The smallest low frequency arc was atmosphere sensitive and can be assigned to the electrode process. Two other arcs are highly depressed and their shapes are not perfect and in some cases left arc is not defined at high frequency. However, some qualitative trends can be concluded from complex impedance plots presented in Fig. 4. It can be seen that only the high frequency arc was strongly dependent on the content of STO in the ceramics. The size of the STO sensitive high frequency arc decreased with increasing temperature and disappeared at 800 °C as shown in Figs. 4 and 5. Another interesting point is that R_1 values obtained by extrapolation seem to be x independent. Therefore, the grain conductivities are as well x independent. This experimental result is consistent with XRD data that showed very limited solubility of STO in CeO_2. However, the incorporation of a small concentration of Sm^{3+} and Ti^{4+} ions into the CeO_2 structure improved the ionic conductivity relative to pure ceria (see Fig. 2). The EDX analysis of $(CeO_2)_{1-x}$–STO_x ceramics revealed 0.6 and 0.4 at.% of samarium and titanium in CeO_2 grains, respectively. SEMs of the microstructures of $(CeO_2)_{1-x}(STO)_x$, for $x = 0$, 0.1, 0.2, after thermal etching at 1200 °C for 24 min is shown in Fig. 6. The average grain size for pure CeO_2 ceramic is 3.6 μm. In general, the microstructure of the STO-doped ceria consists of a low particle size (0.21–0.25 μm) matrix of CeO_2 doped with Sm^{3+} and Ti^{4+} in which randomly distributed clusters of STO, containing a few large (2–5 μm) grains (see Fig. 6d and e), are embedded. It is worth nothing, that presence of STO as a separate phase (due to its limited solubility) remarkably depresses grain growth in the doped ceria matrix (by about one order of magnitude) and the grain growth is x independent on sintering at 1300 °C for 10 h. We note that there are two kinds of the grain boundaries related to the doped-ceria grains in the ceramics, namely, between the ceria–ceria grains and the ceria-STO grains. With increasing STO content the large pyrochlore particles eliminate part of ceria–ceria grain boundaries thereby decreasing the grain-boundary impedance in the range 650–750 °C.

Substantial n-type electronic conductivity was introduced into the system in forming gas via the reduction of Ce^{4+} to Ce^{3+}. It is known that pure CeO_2 (more than 99.99% purity) is a mixed conductor with almost the same partial conductivities of oxygen ion, electron and hole according to Panhans and Blumenthal [16]. The ionic conductivity is significantly increased by the impurity atoms such as Na, Ca, and Sr as is found when a sample of 99.9% purity CeO_2 is used. Ceria shows a n-type conduction at low oxygen partial

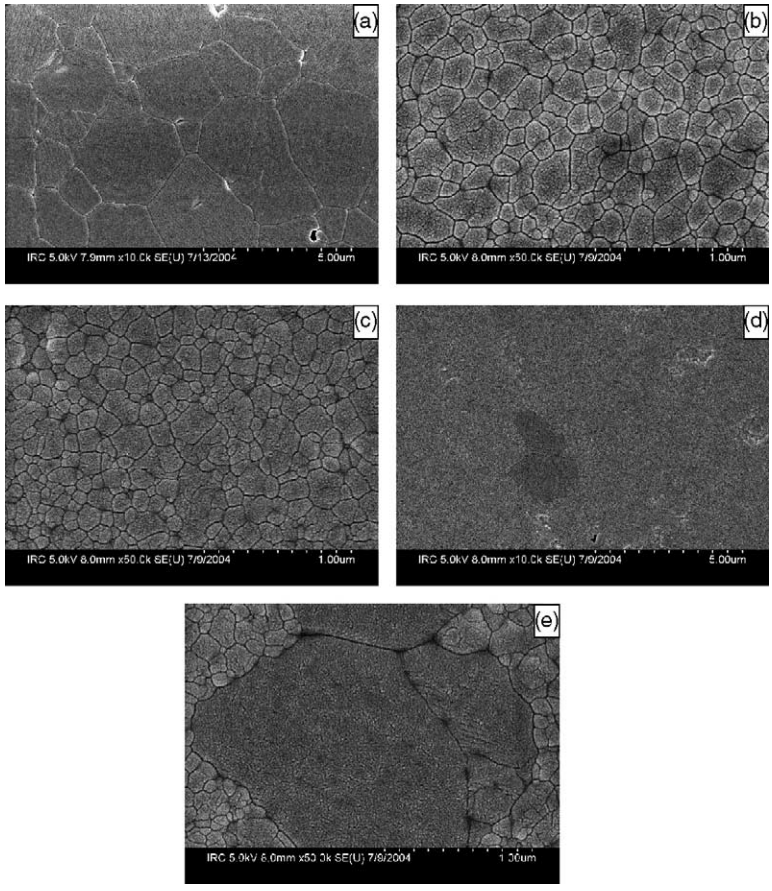

Fig. 6. SEM microstructures of $(CeO_2)_{1-x}(STO)_x$ after thermal etching at 1200 °C for 24 min: (a) $x = 0$, (b) $x = 0.1$, (c) $x = 0.2$, (d and e) $x = 0.2$, the dark STO and light CeO_2 phases were confirmed by EDX.

pressures and high temperature in accordance with equation [15]:

$$O_o = \frac{1}{2}O_2(gas) + V_o^{\bullet\bullet} + 2e \quad (1)$$

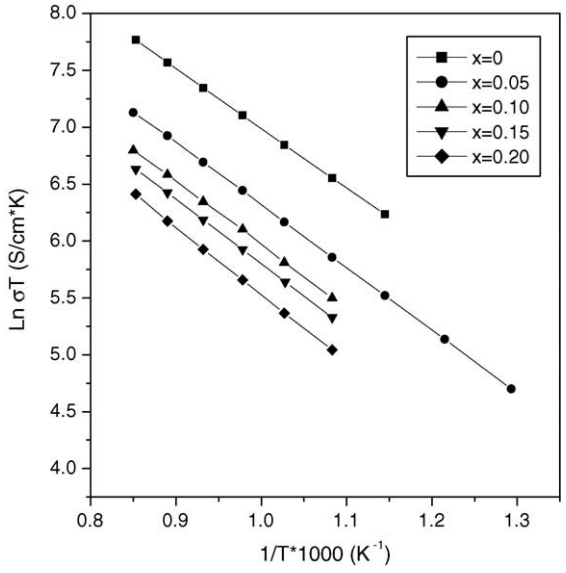

Fig. 7. Conductivity plots $\ln \sigma T$ vs. $1/T$ for $(CeO_2)_{1-x}(STO)_x$ ceramics determined with four-probe method in forming gas (8% H_2–92% Ar).

The presence of electrons moving via a hopping mechanism may be regarded as equivalent to the presence of a Ce^{3+}. Therefore, the total conductivity of pure CeO_2 in reducing atmosphere was higher than that of STO doped CeO_2 and decreased proportionally to the STO content as shown in Fig. 7. The activation energy of STO-containing samples was x independent and very close to the value of pure CeO_2 (see Table 1).

3.2. Thermal expansion depending on temperature and atmosphere

In order to investigate the thermal behavior under reducing condition the ceramics with relatively low density (75–80%) were prepared. The thermal behavior of the CeO_2–STO ceramics was measured in forming gas using a constant heating rate of 3 °C/min up to 900 °C. The samples were held at maximum temperature for 1 h and then cooled down. The results are presented in Fig. 8. The expansion of all ceramics samples was almost the same and x independent in the temperature range of 100–500 °C. A large thermal expansion of $(CeO_2)_{1-x}$–STO_x materials was observed in the range 500–900 °C. The total expansion decreased from 2.75 to 2.4% with increasing content of pyrochlore phase from $x = 0$ to 0.2. The expansion was induced by the reduction of

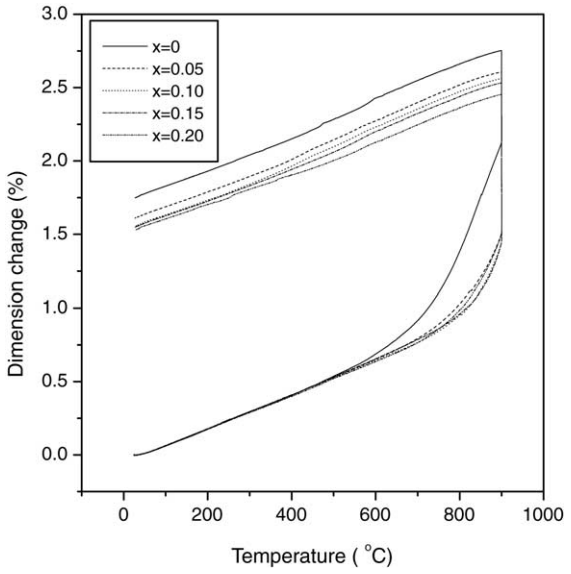

Fig. 8. Dimension change for $(CeO_2)_{1-x}(STO)_x$ ceramics in forming gas (8% H_2–92% Ar) as a function of temperature.

Ce^{4+} to Ce^{3+} and formation of oxygen vacancies. Due to very limited solubility of STO in CeO_2, the contribution of the STO concentration to the total expansion was not significant and the total expansion was governed mainly by the CeO_2 content in ceramics. However, the addition of STO decreased the reduction of CeO_2 and increased the reduction temperature from 500 to 700 °C. The TECs were derived from the cooling stage and were in the range 13×10^{-6} K^{-1} for $x = 0$ to 12×10^{-6} K^{-1} for $x = 0.2$.

3.3. Catalytic activity

Table 2 shows catalytic activities of $(CeO_2)_{1-x}$–STO_x samples towards steam reforming of methane at 900 °C at a S/C (steam/carbon) ratio of 1.8 and a feed rate of 30 cm^3/min. The product distribution under these conditions showed that CO_2 was the main product of CH_4 reforming on the ceria containing catalysts. Reduced CeO_2 powder was found to exhibit relatively low activity for steam reforming of methane under the conditions investigated. In the case of STO additions the catalytic activity increased at $x = 0.05$ and then decreased with further increases in STO composition at $x = 0.1$–0.2. The material with $x = 0.05$ exhibited the highest CO selectivity. The rate of conversion of methane and the CO selectivity decreased with further increases to the STO content. The H_2/CO ratio over the catalyst with $x = 0.2$ was very high, indicating that the water-gas shift reaction

$$CO + H_2O \Leftrightarrow CO_2 + H_2 \quad (2)$$

occurs to an appreciable extent simultaneously with steam reforming. This is due to low methane conversion, which results in the increase of H_2O/CO ratio thus promoting water-gas shift reaction. However, steam reforming of methane and water-gas shift reaction are not the only reactions that can produce hydrogen. Carbon cracking produces hydrogen as well and residual carbons can cause the significant degradation of catalysts. In the case of these experiments, there was no carbon deposition on the catalytic surfaces perhaps because reduced ceria may dissociatively adsorb water [17] and the resulting species can quickly react with carbon species:

$$C + H_2O \Leftrightarrow CO + 2H_2 \quad (3)$$

Furthermore, carbon monoxide can be oxidized on the surface of CeO_2 in accordance with the following reactions:

$$H_2O + Ce_2O_3 \Leftrightarrow 2CeO_2 + H_2 \quad (4)$$

$$CO + 2CeO_2 \Leftrightarrow CO_2 + Ce_2O_3 \quad (5)$$

resulting in increasing H_2/CO ratio [18].

Table 2
Steam reforming of methane on $(CeO_2)_{1-x}(STO)_x$ catalysts[a]

Composition (x)	CH_4 conversion (mol%)	CO/(CO + CO_2) (mol%)	H_2/CO (molar ratio)
0	4	6	53
0.05	10	15	35
0.10	6	8	48
0.15	5	7	43
0.20	4	5	74

[a] Experimental condition: t, 900 °C; H_2O/CH_4, 1.8; feed rate, 30 cm^3/min.

4. Conclusions

Pyrochlore phase $Sm_{0.5}Ti_{0.5}O_{1.75}$ has a very limited solubility in CeO_2. The presence of STO in $(CeO_2)_{1-x}$(-$(STO)_x$ ceramics decreased the magnitude of the grain-boundary effect, and therefore, improved the electrical conductivity in the temperature range of 650–800 °C. The activation energy decreased from 1.86 eV at $x = 0$ to 1.05 eV at $x = 0.2$. Electronic conductivity can be induced in all compositions studied under reducing conditions. The reduction of doped ceramics was lower than that of pure CeO_2 due to partial solubility of STO in ceria. The temperature expansion coefficient under reduced atmosphere for mixed ceramics decreased from 13×10^{-6} to 12×10^{-6} K^{-1} as x increased from 0 to 0.2.

The $(CeO_2)_{1-x}(STO)_x$ ceramics were catalytically active for steam reforming of methane. The material with $x = 0.05$ showed the highest catalytic activity towards steam methane reforming at 900 °C. $(CeO_2)_{1-x}(STO)_x$ compositions exhibited a high mixed conductivity and were catalytically active with a lower TEC than pure CeO_2 under reducing conditions. Therefore, STO doped CeO_2 ceramics may be considered as the ceramic component in cermet or ceramic anode in SOFCs.

Acknowledgments

This work was partially supported by a joint collaborative research project with Global Thermoelectric Inc. The authors wish to thank Jim Margeson for SEM and EDX analyses.

References

[1] B.C.H. Steele, P.H. Middleton, R.A. Rudkin, Material science aspects of SOFC technology with special reference to anode development, Solid State Ionics 40/41 (1990) 388–393.

[2] O.A. Marina, L.R. Pederson, Novel ceramic anodes for SOFCs tolerant to oxygen, carbon and sulfur, in: J. Huijsmans (Ed.), in: Proceedings of the Fifth European SOFC Forum, Lucerne, Switzerland, 2002, pp. 481–489.

[3] O.A. Marina, C. Bagger, S. Primdahl, M. Mogensen, A solid oxide fuel cell with a gadolinia-doped ceria anode: preparation and performance, Solid State Ionics 123 (1999) 199–208.

[4] H. Yahiro, K. Eguchi, H. Arai, Electrical properties and reducibilities of ceria–rare earth oxide systems and their application to solid oxide fuel cell, Solid State Ionics 36 (1989) 71–75.

[5] E.P. Murray, T. Tsai, S.A. Barnett, A direct-methane fuel cell with a ceria-based anode, Nature 400 (1999) 649–651.

[6] O.A. Marina, M. Mogensen, High-temperature conversion of methane on a composite gadolinia-doped ceria–gold electrode, Appl. Catal. A189 (1999) 117–126.

[7] T. Bunluesin, R.J. Gorte, G.W. Graham, Studies of the water-gas-shift reaction on ceria-supported Pt, Pd, and Rh: implications for oxygen-storage properties, Appl. Catal. B15 (1998) 107–114.

[8] M. Mogensen, T. Lindegaard, U.R. Hansen, G. Mogensen, Physical properties of mixed conductor solid oxide fuel cell anodes of doped CeO_2, J. Electrochem. Soc. 141 (1994) 2122–2128.

[9] F.M. Figueriredo, J.R. Frade, F.M.B. Marques, Electrical and electrochemical behavior of $LaCoO_{3-\delta} + La_2(Zr,Y)_2O_7$-based electrode materials, Solid State Ionics 118 (1999) 81–87.

[10] A.T. Ashcroft, A.K. Cheetham, J.S. Foord, M.L.H. Green, C.P. Grey, A.J. Murrell, P.D.F. Vernon, Selective oxidation of methane to synthesis gas using transition metal catalysts, Nature 344 (1990) 319–321.

[11] M.I. Mendelson, Average grain size in polycrystalline ceramics, J. Am. Ceram. Soc. 52 (8) (1969) 443–446.

[12] International Center for Diffraction Data, file 78-0694.

[13] M.J. Verkerk, B.J. Middelhuis, A.J. Burggraaf, Effect of grain boundaries on the conductivity of high-purity ZrO_2–Y_2O_3 ceramics, Solid State Ionics 6 (1982) 159–170.

[14] D.Y. Wang, A.S. Nowick, The ''grain-boundary effect'' in doped ceria solid electrolytes, J. Solid. State Chem. 35 (1980) 325–333.

[15] H.L. Tuller, A.S. Nowick, Doped ceria as a solid oxide electrolyte, J. Electrochem. Soc. 122 (1975) 255–259.

[16] M.A. Panhans, R.N. Blumenthal, A thermodynamic and electrical conductivity study of nonstoichiometric cerium dioxide, Solid State Ionics 60 (1993) 279–298.

[17] Q. Zhuang, Y. Qin, L. Chang, Promotion effect of cerium oxide in supported nickel catalyst for hydrocarbon steam-reforming, Appl. Catal. 70 (1991) 1–8.

[18] K. Otsuka, M. Hatano, A. Morikawa, Hydrogen from water by reduced cerium oxide, J. Catal. 79 (1983) 493–496.